

Anisotropic Fretting Wear Simulation Using the Boundary Element Method

L. Rodríguez-Tembleque¹, R. Abascal¹ and M.H. Aliabadi²

Abstract: A boundary element based formulation is proposed to simulate 3D fretting wear under gross-sliding and partial slip conditions, assuming anisotropic friction and wear laws. Contact problem is based on an *Augmented Lagrangian formulation*, and restrictions fulfilment is established by a set of projection functions. The boundary element method reveals to be a very suitable numerical method for this kind of problems, where the degrees of freedom involved are those on the solids surfaces, and a very good approximation on contact tractions is obtained with a low number of elements. The present boundary element anisotropic fretting wear formulation is illustrated with some examples, in which some studies about the influence of anisotropy on fretting wear are presented.

Keywords: Anisotropic wear, Fretting wear, Contact, Anisotropic friction, Boundary element, Fretting.

1 Introduction

The prediction of wear is a significant issue for the design of mechanical components. Many engineering assemblies contains contacting components subject to a small amplitude oscillatory relative movement, and the damage on the surfaces that results from these fretting conditions can cause important reduction in useful life. So the economic implication of wear prediction can be of enormous value to the industry.

Many researchers have been studied this phenomenon since the end of the first half of the twentieth century. It must be emphasized the important contributions of [Holm (1946)] and [Archard (1953)], as well as the works of [Rabinowicz (1995)]. In the last twenty years, many researchers have proposed different analytic and semi-analytic models to predict wear on fretting problems: [Hills and Nowell

¹ Escuela Técnica Superior de Ingeniería, Universidad de Sevilla, Camino de los Descubrimientos s/n , Sevilla E-41092, Spain.

² Department of Aeronautics, Imperial College London, London, SW7 2AZ, UK

(1994)] and [Goryacheva, Rajeev, and Farris (2001)], [Hills, Sackfield, and Paynter (2009)] and [Nowell (2010)] have to be mentioned. Numerical formulations have also been developed in the last years using different methodologies. On contact problems using the Finite Element Method (FEM), it has to be mentioned the fundamental works of [Johansson (1994)], [Strömberg, Johansson, and Klarbring (1996)] and [Strömberg (1997, 1999)], and more recently [Ireman, Klarbring, and Strömberg (2003, 2009)], which present the formulations and fundamentals for wear simulations. [Pödra and Andersson (1999b,a)] present a sliding wear algorithm based on a FEM commercial code, [McColl, Ding, and Leen (2004)] present a 2D finite element-based method for simulating fretting wear compared with experimental measurements and [Madge, Leen, and Shipway (2007)] propose a 2D finite element model for fretting fatigue. More recently, it has to be mentioned the numerical and experimental wear analysis presented by [Paczelt, Kucharski, and Mróz (2012)] and [Paczelt and Mróz (2012)].

On the boundary element area, the number of works related with wear is increasing in the last years due to the fact that the Boundary Element Method (BEM) proves to be a suitable numerical formulation for this kind of mechanical interaction problems, in which it is necessary to reduce the CPU times and obtain good accuracy of the contact variables. It has to be mentioned the works of [Sfantos and Aliabadi (2006a,b,c, 2007)], [Lee, Tian, Bae, and Chai (2009)], [Kim, Moon, and Cho (2011)], and recently the contributions presented by the authors [Rodríguez-Tembleque, Abascal, and Aliabadi (2010, 2011)].

The contact models mentioned above are based on isotropic tribological properties where friction is assumed to be constant and modeled using the isotropic Coulomb law, and wear models are also based on an isotropic wear law [Holm (1946); Archard (1953)]. This is true when the contact surfaces present an isotropic roughness. However, in a great number of engineering applications, the distribution of the asperities and hollows on the surfaces are not identical on every point. In these cases, friction and wear properties depend on the sliding direction, so an anisotropic friction and wear laws have to be considered. Particularly, in a large number of machining processes, the striations are mutually orthogonal. For such cases, an orthotropic friction and wear laws must be considered. Some works in the literature have studied and developed different friction models, which define the admissible region for contact tractions (*Friction Cone*) and the sliding rules. [Curnier (1984)] presents a general theory of friction, [Michalowski and Mróz (1978)] and [Mróz and Stupkiewicz (1994)] consider an orthotropic model with a non-associated sliding rule, and [Zmitrowicz (1989, 1999, 2006a, 2010)] takes into account more sophisticated friction models.

Analytical solutions for some isotropic frictional contact problems can be found in

the literature [Johnson (1985); Hills, Nowell, and Sackfield (1993)], whereas this is not so for anisotropic frictional contact cases involving more realistic friction models such as the ones mentioned in the previous paragraph. Hence the need to resort to numerical resolutions such as the ones proposed by [Buczowski and Kleiber (1997, 2009)] and [Zhang, He, Li, and Wriggers (2004)], who present a 3D elastoplastic interface formulation for orthotropic frictional problems. [Jones and Papadopoulos (2006)] develop a constitutive description and numerical formulation for more general anisotropic descriptions, and [Konyukhov and Schweizerhof (2006)] for anisotropic in adhesion and frictional problems. [Hjiaj, de Saxcé, and Mróz (2002); Hjiaj, Feng, de Saxcé, and Mróz (2004)], and [Feng, Hjiaj, de Saxcé, and Mróz (2006a,b)] present a numerical formulation for orthotropic frictional contact problems with a non-associated sliding rule, and an algorithm for resolution based on a bi-potential framework [de Saxcé and Feng (1991)] and [Joli and Feng (2008)]. Those formulations show the importance of the tangential contact variables approximation and the difficulties involved in the anisotropic friction law fulfilment, during the resolution process.

Anisotropic wear constitutive models can be found in the literature [Zmitrowicz (1993), Zmitrowicz (2006b)], whereas this is not so for numerical formulations considering anisotropic tribological properties, specially in fretting wear conditions. This work presents a boundary element based formulation for modeling anisotropic fretting wear problems. The contact problem is formulated by means of the augmented Lagrangian similarly to [Alart and Curnier (1991)], [Klarbring (1992, 1993)], [Strömberg, Johansson, and Klarbring (1996)] and [Strömberg (1997, 1999)], [Christensen, Klarbring, Pang, and Strömberg (1998)], [González and Abascal (1998, 2000, 2002)], [Abascal and Rodríguez-Tembleque (2007)], [González, Park, Felippa, and Abascal (2008)], [Rodríguez-Tembleque and Abascal (2010a,b, 2012)]. Another recent formulations, like the interesting contact methodology presented by [Oliver, Hartmann, Cante, Weyler, and Hernández (2009)], [Hartmann, Oliver, Weyler, Cante, and Hernández (2009)] and [Hartmann, Weyler, Oliver, Cante, and Hernández (2010)], are not considered in this work due to the difficulties associated to orthotropic friction law fulfilment in anisotropic wear conditions. The material loss of the bodies under fretting wear conditions is modeled using a wear law based on [Zmitrowicz (1993, 2006b)]. These works suggest that the material removed per time unit is a function of the normal pressure and the sliding velocity with a wear intensity coefficient, and this coefficient is an intensity function depending on the sliding direction, so the material removed is dependent on the sliding direction.

The document starts presenting the anisotropic contact and wear models in Section 2 and Section 3, respectively. Section 4 deals with the boundary element equations

and the discrete anisotropic frictional contact and fretting wear governing equations. In Section 5, an Uzawa (predictor-corrector) scheme is proposed. Finally, the proposed methodology is applied in Section 6 to solve fretting wear problems under gross sliding and partial slip conditions. The results show that anisotropic tribological properties have a significant effect on the contact variables and wear evolution in fretting problems.

2 Modeling Contact

The contact problem between two solids Ω^α ($\alpha = 1, 2$), with boundaries Γ^α , defined in a Cartesian coordinate system: $x_i \equiv \{x_1, x_2, x_3\}$ on \mathbb{R}^3 (see Fig.1), is considered. In order to know the relative position between both bodies at all times (τ), a gap variable is defined for the pair $I \equiv \{P^1, P^2\}$ of points ($P^\alpha \in \Omega^\alpha, \alpha = 1, 2$), as

$$\mathbf{g} = \mathbf{B}^T(\mathbf{x}^2 - \mathbf{x}^1) \tag{1}$$

where \mathbf{x}^α is the position of P^α at every instant, defined as: $\mathbf{x}^\alpha = \mathbf{X}^\alpha + \mathbf{u}_o^\alpha + \mathbf{u}^\alpha$ (\mathbf{X}^α : global position; \mathbf{u}_o^α : rigid body global displacement; \mathbf{u}^α : elastic displacement expressed in the global system). Matrix $\mathbf{B} = [\mathbf{e}_1 | \mathbf{e}_2 | \mathbf{n}]$, is a base change matrix expressing the pair I gap in relation to the local orthonormal base $\{\mathbf{e}_1, \mathbf{e}_2, \mathbf{n}\}$ associated to every I pair. The unitary vector \mathbf{n} is normal to the contact surfaces with the same direction as the normal to Γ^1 and expressed in the global system. Vectors $\{\mathbf{e}_1, \mathbf{e}_2\}$ are the tangential unitarian vectors.

The expression (1) can be written as: $\mathbf{g} = \mathbf{B}^T(\mathbf{X}^2 - \mathbf{X}^1) + \mathbf{B}^T(\mathbf{u}_o^2 - \mathbf{u}_o^1) + \mathbf{B}^T(\mathbf{u}^2 - \mathbf{u}^1)$, $\mathbf{B}^T(\mathbf{X}^2 - \mathbf{X}^1)$ being the *geometric gap* between two solids in the reference configuration (\mathbf{g}_g), and $\mathbf{B}^T(\mathbf{u}_o^2 - \mathbf{u}_o^1)$ the gap originated due to the *translation* (\mathbf{g}_o). Therefore, the gap of the I pair remains as follows:

$$\mathbf{g} = \mathbf{g}_{g_o} + \mathbf{B}^T(\mathbf{u}^2 - \mathbf{u}^1) \tag{2}$$

where $\mathbf{g}_{g_o} = \mathbf{g}_g + \mathbf{g}_o$. In this work, the reference configuration for each solid (\mathbf{X}^α) that will be considered is the initial configuration (before applying load). Consequently, \mathbf{g}_g may also be termed *initial geometric gap*. In the expression (2) two components can be identified: the normal gap, $g_n = g_{g_o,n} + u_n^2 - u_n^1$, and the tangential gap or *slip*, $\mathbf{g}_t = \mathbf{g}_{g_o,t} + \mathbf{u}_t^2 - \mathbf{u}_t^1$, u_n^α and \mathbf{u}_t^α being the normal and tangential displacements, respectively.

2.1 Unilateral contact law

The unilateral contact law involves two conditions [Wriggers (2002)] and [Laursen (2002)]: impenetrability and no cohesion. The bodies Ω^α ($\alpha = 1, 2$) present no interpenetration: $\Omega^1 \cap \Omega^2 = \emptyset$. Therefore, the surface of each body can be divided

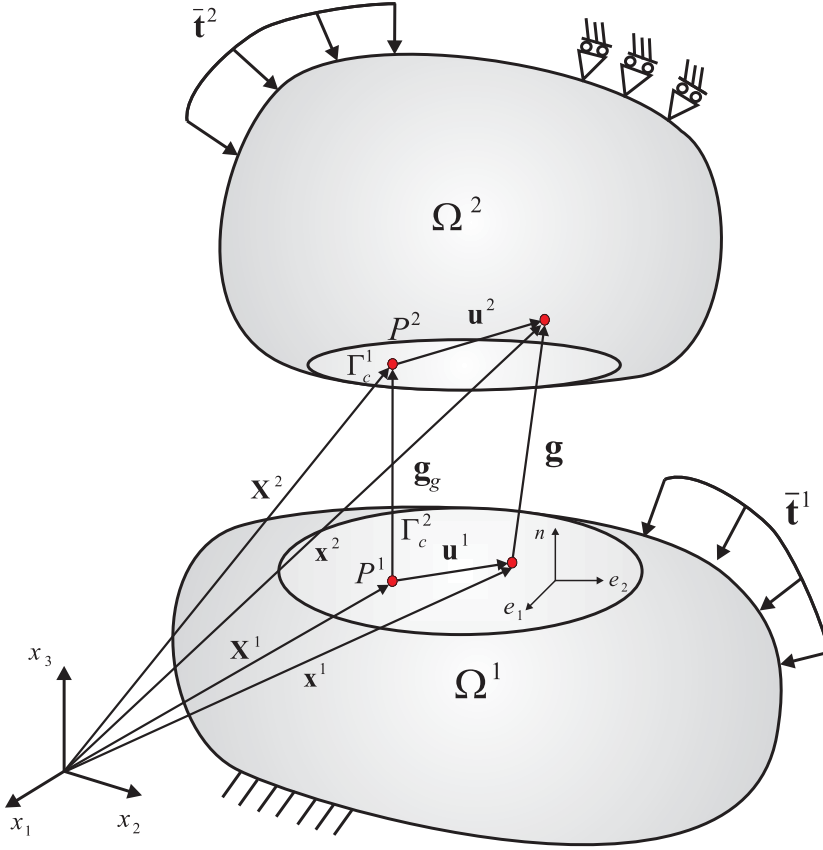


Figure 1: Contact pair I of points $P^\alpha \in \Omega^\alpha$ ($\alpha = 1, 2$).

in three regions depending on whether it is in contact (Γ_c^α), with imposed tractions (Γ_t^α) or with imposed displacements (Γ_u^α), so that: $\Gamma^\alpha = \Gamma_c^\alpha \cup \Gamma_u^\alpha \cup \Gamma_t^\alpha$ and $\Gamma_c^\alpha \cap \Gamma_u^\alpha \cap \Gamma_t^\alpha = \emptyset$, with $\alpha = 1, 2$. Moreover it is possible to denote the *Contact Zone* as Γ_c , since: $\Gamma_c \simeq \Gamma_c^1 \simeq \Gamma_c^2$.

The solids are in contact without cohesion, they can be separated, therefore for each pair $I \equiv \{P^1, P^2\} \in \Gamma_c$: $g_n \geq 0$ and $t_n \leq 0$. The variable g_n is the pair I normal gap, and t_n is the normal contact traction defined as: $t_n = \mathbf{B}_n^T \mathbf{t}^1 = -\mathbf{B}_n^T \mathbf{t}^2$, where \mathbf{t}^α is the traction of point $P^\alpha \in \Gamma_c^\alpha$ expressed in the global system of reference, and $\mathbf{B}_n = [\mathbf{n}]$ is the third column in the change of base matrix: $\mathbf{B} = [\mathbf{B}_i | \mathbf{B}_n] = [\mathbf{e}_1 | \mathbf{e}_2 | \mathbf{n}]$. Tangential traction is defined as: $\mathbf{t}_t = \mathbf{B}_t^T \mathbf{t}^1 = -\mathbf{B}_t^T \mathbf{t}^2$. Both tractions, \mathbf{t}^1 and \mathbf{t}^2 have

the same value and opposite signs, in accordance with Newton’s third law.

Finally, the variables g_n and t_n are complementary: $g_n t_n = 0$, so this set of relations may be summarized on Γ_c by the so-called Signorini conditions:

$$g_n \geq 0, \quad t_n \leq 0, \quad g_n t_n = 0 \tag{3}$$

which has to be satisfied at each instant τ .

2.2 Orthotropic friction law

Experimental observations concerned with the directional sliding effects in anisotropic friction were provided by [Rabinowicz (1957)], [Halaunbrenner (1960)], and [Minford and Prewo (1985)], while theoretical investigations on friction surfaces and sliding rules have been carried out by [Mróz and Stupkiewicz (1994)] and [Zmitrowicz (1989, 1999)]. Their studies show that, in general, cross sections of the friction cone could be non-convex. However, in many engineering applications, a family of anisotropic friction models can be accurately approximated by a convex elliptical friction cone. The principal axes of the ellipse coincide with the orthotropic axes (Fig. 2(a)). The generic form of such anisotropic limit friction is given by

$$f(\mathbf{t}_t, t_n) = \|\mathbf{t}_t\|_\mu - |t_n| = 0 \tag{4}$$

where $\|\bullet\|_\mu$ denotes the elliptic norm

$$\|\mathbf{t}_t\|_\mu = \sqrt{\left(\frac{t_{e_1}}{\mu_1}\right)^2 + \left(\frac{t_{e_2}}{\mu_2}\right)^2} \tag{5}$$

and the coefficients μ_1 and μ_2 are the principal friction coefficients in the directions $\{e_1, e_2\}$. Curve (4) constitutes an ellipse whose principal axes are: $\mu_1 |t_n|$ and $\mu_2 |t_n|$ (see Fig. 2(b)). The classical isotropic Coulomb’s friction criterion is recovered on curve (4) considering $\mu_1 = \mu_2 = \mu$. The allowable contact tractions \mathbf{t} must satisfy: $f(\mathbf{t}_t, t_n) \leq 0$, defining an admissible convex region for \mathbf{t} : the *Friction Cone* (\mathbb{C}_f).

An associated sliding rule is considered, so the sliding direction is given by the gradient to the friction cone and its magnitude by the factor λ :

$$\dot{g}_{e_1} = -\lambda \frac{\partial f}{\partial t_{e_1}} = -\frac{\lambda}{\mu_1^2} \frac{t_{e_1}}{\|\mathbf{t}_t\|_\mu} \tag{6}$$

$$\dot{g}_{e_2} = -\lambda \frac{\partial f}{\partial t_{e_2}} = -\frac{\lambda}{\mu_2^2} \frac{t_{e_2}}{\|\mathbf{t}_t\|_\mu} \tag{7}$$

To satisfy the complementarity relations

$$f(\mathbf{t}_t, t_n) \leq 0, \quad \lambda \geq 0, \quad \lambda f(\mathbf{t}_t, t_n) = 0 \tag{8}$$

the expression for λ factor is: $\lambda = \|\dot{\mathbf{g}}_t\|_\mu^*$, where the norm $\|\bullet\|_\mu^*$ is dual of $\|\bullet\|_\mu$, so: $\|\dot{\mathbf{g}}_t\|_\mu^* = \sqrt{(\mu_1 \dot{g}_{e_1})^2 + (\mu_2 \dot{g}_{e_2})^2}$. Thus

$$t_{e_1} = -\|\mathbf{t}_t\|_\mu \frac{\mu_1^2 \dot{g}_{e_1}}{\|\dot{\mathbf{g}}_t\|_\mu^*} \quad (9)$$

$$t_{e_2} = -\|\mathbf{t}_t\|_\mu \frac{\mu_2^2 \dot{g}_{e_2}}{\|\dot{\mathbf{g}}_t\|_\mu^*} \quad (10)$$

From (9) and (10) we can derive the following relation

$$\frac{t_{e_2}}{t_{e_1}} = \left(\frac{\mu_2}{\mu_1}\right)^2 \frac{\dot{g}_{e_2}}{\dot{g}_{e_1}} \quad (11)$$

Let θ_t and θ_g denote the inclination angles of the tangential traction and slip, respectively. Then (11) becomes

$$\tan\theta_t = \left(\frac{\mu_2}{\mu_1}\right)^2 \tan\theta_g \quad (12)$$

which indicates that the direction of tangential contact traction can be different from the slip direction, according to the anisotropic friction law.

2.3 Anisotropic contact restrictions

The *unilateral contact condition* and the *elliptic friction law* defined for any pair $I \equiv \{P^1, P^2\} \in \Gamma_c$ of points in contact can be compiled as follows, according to their contact status:

$$\text{No contact :} \quad g_n \geq 0, \quad t_n = 0, \quad \mathbf{t}_t = \mathbf{0}$$

$$\text{Contact-Adhesion:} \quad g_n = 0, \quad t_n \leq 0, \quad \dot{\mathbf{g}}_t = \mathbf{0} \quad (13)$$

$$\text{Contact-Slip:} \quad g_n = 0, \quad t_n \leq 0, \quad \mathbf{t}_t = -|t_n| \mathbb{M}^2 \dot{\mathbf{g}}_t / \|\dot{\mathbf{g}}_t\|_\mu^*$$

being

$$\mathbb{M} = \begin{bmatrix} \mu_1 & 0 \\ 0 & \mu_2 \end{bmatrix} \quad (14)$$

In the expressions (13), $\dot{\mathbf{g}}_t$ is the tangential slip velocity which can be expressed at time τ_k as: $\dot{\mathbf{g}}_t \simeq \Delta \mathbf{g}_t / \Delta \tau$, where $\Delta \mathbf{g}_t = \mathbf{g}_t(\tau_k) - \mathbf{g}_t(\tau_{k-1})$ and $\Delta \tau = \tau_k - \tau_{k-1}$, according to a standard backward Euler scheme.

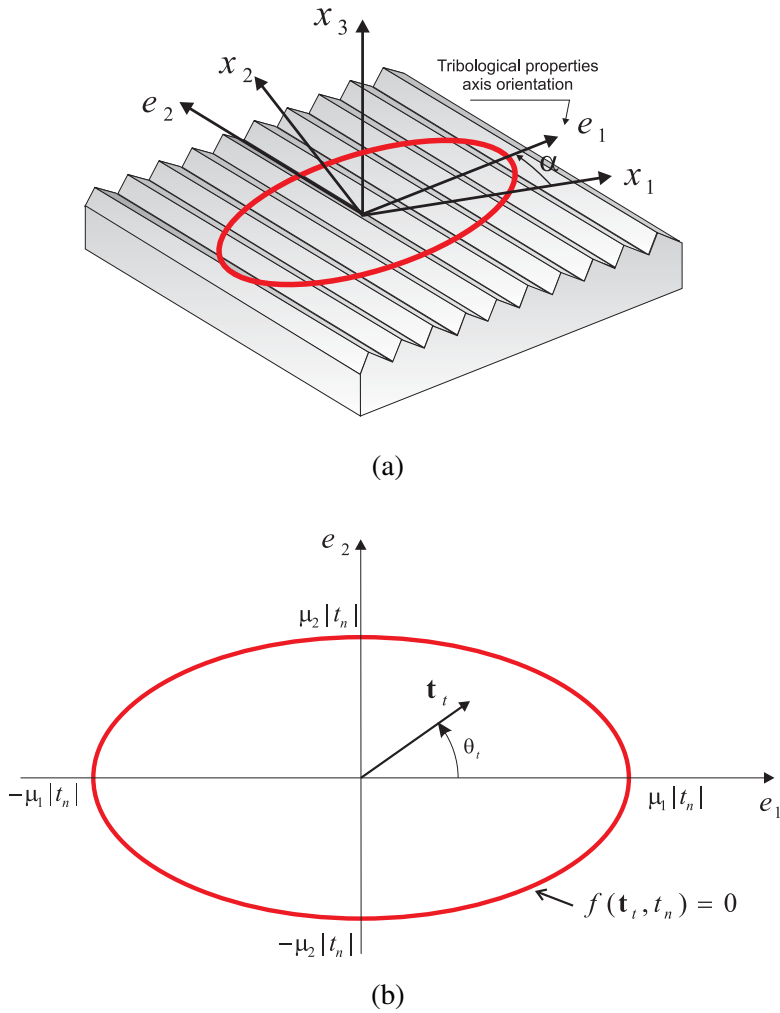


Figure 2: (a) Orthotropic surface with parallel wedge asperities. (b) Elliptic friction law.

The constraints of the combined normal-tangential contact problem (13) can be formulated as

$$\mathbf{t} - \mathbb{P}_{\mathbb{C}_f}(\mathbf{t}^*) = \mathbf{0} \quad (15)$$

where the contact operator $\mathbb{P}_{\mathbb{C}_f}$ is defined as

$$\mathbb{P}_{\mathbb{C}_f}(\mathbf{t}^*) = \left\{ \begin{array}{l} \mathbb{P}_{\mathbb{E}_\rho}(\mathbf{t}_t^*) \\ \mathbb{P}_{\mathbb{R}_-}(t_n^*) \end{array} \right\} \quad (16)$$

The normal projection function, $\mathbb{P}_{\mathbb{R}_-}(\cdot) : \mathbb{R} \longrightarrow \mathbb{R}_-$, is defined as

$$\mathbb{P}_{\mathbb{R}_-}(x) = \min(x, 0) \quad (17)$$

and the tangential projection function, $\mathbb{P}_{\mathbb{E}_\rho}, \mathbb{P}_{\mathbb{E}_\rho}(\cdot) : \mathbb{R}^2 \longrightarrow \mathbb{R}^2$,

$$\mathbb{P}_{\mathbb{E}_\rho}(\mathbf{x}) = \left\{ \begin{array}{ll} \mathbf{x} & \text{if } \|\mathbf{x}\|_\mu < \rho \\ \rho \mathbf{e}_t & \text{if } \|\mathbf{x}\|_\mu \geq \rho \quad (\mathbf{e}_t = \mathbf{x}/\|\mathbf{x}\|_\mu) \end{array} \right. \quad (18)$$

with $\mathbb{E}_\rho = \{\mathbf{x} \in \mathbb{R}^2 : \|\mathbf{x}\|_\mu - \rho = 0\}$ ($\rho = |\mathbb{P}_{\mathbb{R}_-}(t_n^*)|$). The augmented traction components $(\mathbf{t}^*)^T = [(t_t^*)^T t_n^*]$ are defined as:

$$\mathbf{t}_t^* = \mathbf{t}_t - r_t \mathbb{M}^2 \Delta \mathbf{g}_t \quad (19)$$

$$t_n^* = t_n + r_n g_n \quad (20)$$

being r_n and r_t the normal and tangential dimensional penalization parameters ($r_n \in \mathbb{R}^+, r_t \in \mathbb{R}^+$), respectively.

The expression (15) compiles the unilateral contact law and orthotropic friction criterion, taking into account the contact status of every pair I :

- $(t_n^*)_I > 0$ (No Contact): $(\mathbf{t})_I = \mathbf{0}$
- $(t_n^*)_I \leq 0$ (Contact):
 - $\|(t_t^*)_I\|_\mu < |\mathbb{P}_{\mathbb{R}_-}((t_n^*)_I)|$ (Adhesion): $\left\{ \begin{array}{l} \Delta \mathbf{g}_t \\ g_n \end{array} \right\}_I = \mathbf{0}$
 - $\|(t_t^*)_I\|_\mu \geq |\mathbb{P}_{\mathbb{R}_-}((t_n^*)_I)|$ (Slip): $\left\{ \begin{array}{l} \mathbf{t}_t - |t_n^*| \boldsymbol{\omega}_t^* \\ g_n \end{array} \right\}_I = \mathbf{0}$

being $\boldsymbol{\omega}_t^* = \mathbf{t}_t^* / \|\mathbf{t}_t^*\|_\mu$.

3 Modeling anisotropic wear

The Holm-Archard's wear law Rabinowicz (1995) allows to compute the total volume of solid particles worn (W) as

$$W = k_w \frac{F_n}{H} D_s \tag{21}$$

where F_n is the contact normal load, H is the surface hardness, D_s is the sliding distance, and k_w is the nondimensional wear coefficient, which represents the probability of forming a substantial wear particle (by interpretation of Archard). Expression (21) can be written locally for an infinitesimally small apparent contact area as

$$g_w = i_w |t_n| D_s \tag{22}$$

g_w being the wear depth, t_n the normal contact pressure, and $i_w = k_w/H$ the dimensional wear coefficient or the specific wear rate. Wear process evolves over time, so equation (22) might be expressed in a differential form. Particularly, in a steady wear state, this wear evolution can be expressed in the following wear rate form

$$\dot{g}_w = i_w |t_n| \dot{D}_s \tag{23}$$

where \dot{D}_s is the tangential slip velocity module: $\dot{D}_s = \|\dot{\mathbf{g}}_t\|$.

Anisotropic wear is induced by anisotropic friction, according to Zmitrowicz (1993, 2006b). Anisotropic friction results from anisotropic distribution of the asperities and hollows on the contacting surfaces and/or anisotropy of mechanical properties of materials. Assuming that the wear intensity i_w is a function of the sliding direction parameter α_v ($i_w = i_w(\alpha_v)$), wear velocity (\dot{g}_w) depends on the sliding direction. α_v is the measure of the oriented angle between the given direction (\mathbf{e}_1) and the sliding velocity direction.

Let us consider an orthotropic wear law,

$$i_w(\alpha_v) = \sqrt{(i_1 \cos \alpha_v)^2 + (i_2 \sin \alpha_v)^2} \tag{24}$$

where: $\cos \alpha_v = \dot{g}_{e_1} / \|\dot{\mathbf{g}}_t\|$, $\sin \alpha_v = \dot{g}_{e_2} / \|\dot{\mathbf{g}}_t\|$, and i_1 and i_2 are the principal intensity coefficients. Postulating the wear rate to be proportional to the friction dissipation energy makes $i_1 = k\mu_1|t_n|$ and $i_2 = k\mu_2|t_n|$, so they are related to friction coefficients through the wear factor k . Developing expression (24), the wear intensity can be written as

$$i_w = \frac{\|\dot{\mathbf{g}}_t\|_i}{\|\dot{\mathbf{g}}_t\|} \tag{25}$$

being $\|\dot{\mathbf{g}}_t\|_i = \sqrt{(i_1 \dot{g}_{e_1})^2 + (i_2 \dot{g}_{e_2})^2}$. So the anisotropic wear law (23) is defined by

$$\dot{g}_w = |t_n| \|\dot{\mathbf{g}}_t\|_i \quad (26)$$

For quasi-static contact problems, wear depth defined on instant τ_k , is computed as

$$g_w = g_w(\tau_{k-1}) + |t_n| \|\Delta \mathbf{g}_t\|_i \quad (27)$$

t_n and $\Delta \mathbf{g}_t$ being the normal contact pressure and the sliding distance ($\Delta \mathbf{g}_t = \mathbf{g}_t(\tau_k) - \mathbf{g}_t(\tau_{k-1})$), respectively, calculated on the same instant, and $g_w(\tau_{k-1})$ the wear depth value on instant τ_{k-1} . Wear depth on each solid surface is computed from the total wear depth g_w as

$$g_w^1 = \frac{g_w}{1 + (i_w^2/i_w^1)} \quad g_w^2 = \frac{g_w}{1 + (i_w^1/i_w^2)} \quad (28)$$

so: $g_w = g_w^1 + g_w^2$. In the expression above i_w^α ($\alpha = 1, 2$) is the solid Ω^α wear coefficient.

Due to the fact that the depth of removed material is computed for an instant τ_k , the normal contact gap (g_n) at the same time must be rewritten:

$$g_n = g_{go,n} + (u_n^2 - u_n^1) + g_w \quad (29)$$

4 Discrete equations

4.1 Boundary element equations

The BEM proves to be a very suitable numerical method to approximate the elastic response of solids under contact conditions, due to the good approximation of contact tractions with a low number of elements. The BEM formulation for an elastic continuum Ω with boundary Γ is well known and can be found in many classical texts such as Brebbia and Dominguez (1992); Aliabadi (2002). For a boundary point ($P \in \Gamma$), the *Somigliana identity* can be written as:

$$\mathbf{C} \mathbf{u}(P) + CPV \left\{ \int_{\Gamma} \mathbf{T}^* \mathbf{u} \, d\Gamma \right\} = \int_{\Omega} \mathbf{U}^* \mathbf{b} \, d\Omega + \int_{\Gamma} \mathbf{U}^* \mathbf{t} \, d\Gamma \quad (30)$$

where \mathbf{u} , \mathbf{t} and \mathbf{b} are, respectively, the displacements, the boundary tractions and the body forces of Ω . $\mathbf{U}^* = \{U_{lm}^*(P, Q)\}$ is the fundamental solution tensor for displacement (free-space Green's functions), and $\mathbf{T}^* = \{T_{lm}^*(P, Q)\}$ stands for tractions fundamental solution, at point Q in the l th direction, due to a unit load applied at point P in the m th direction. Matrix \mathbf{C} is equal to $\frac{1}{2} \mathbf{I}$ for a smooth boundary Γ , and $CPV \{ \int \cdot d\Gamma \}$ denotes the *Cauchy Principal Value* of the integral $\int \cdot d\Gamma$.

The boundary Γ is divided into N_e elements, $\Gamma^e \in \Gamma$, so: $\Gamma = \bigcup_{e=1}^{N_e} \Gamma^e$ and $\bigcap_{e=1}^{N_e} \Gamma^e = \emptyset$. The fields \mathbf{u} and \mathbf{t} are approximated over each element Γ^e using shape functions, as a function of the nodal values (\mathbf{d}^e and \mathbf{p}^e): $\mathbf{u} \simeq \hat{\mathbf{u}} = \mathbf{N}\mathbf{d}^e$ and $\mathbf{t} \simeq \hat{\mathbf{t}} = \mathbf{N}\mathbf{p}^e$, \mathbf{N} being the shape functions approximation matrix. So the discrete expression for the integral equation (30) can be written, in absence of body loads ($\mathbf{b} = \mathbf{0}$), as follows:

$$\mathbf{C}_i \mathbf{u}_i + \sum_{e=1}^N \mathbf{H}_i^e \mathbf{d}^e = \sum_{e=1}^N \mathbf{G}_i^e \mathbf{p}^e \tag{31}$$

being: $\mathbf{H}_i^e = \int_{\Gamma^e} \mathbf{T}^* \mathbf{N} d\Gamma$; $\mathbf{G}_i^e = \int_{\Gamma^e} \mathbf{U}^* \mathbf{N} d\Gamma$, the integrals over the element e when the collocation point is the node i , and \mathbf{C}_i is the *free term* matrix, according to Brebbia and Dominguez (1992); Aliabadi (2002). Finally, the contribution for all i nodes can be written together in matrix form, resulting in the global system of equations: $\mathbf{H}\mathbf{d} = \mathbf{G}\mathbf{p}$, where \mathbf{d} and \mathbf{p} are the nodal displacements and tractions vectors, respectively. Matrices \mathbf{G} and \mathbf{H} are constructed collecting the terms of matrices \mathbf{H}_i^e and \mathbf{G}_i^e . Boundary conditions can be imposed rearranging the columns in \mathbf{H} and \mathbf{G} , and passing all the unknowns to vector \mathbf{x} on the left-hand side, resulting in the final system

$$\mathbf{A}\mathbf{x} = \mathbf{F} \tag{32}$$

4.2 Contact variables

To consider the contact between two solids, the contact tractions (\mathbf{t}_c), the gap (\mathbf{g}), and the displacements (\mathbf{u}^α , $\alpha = 1,2$), are discretized over the contact interface (Γ_c). To that end, Γ_c is divided into N^f elemental surfaces (Γ_c^e), thus $\Gamma_c = \bigcup_{e=1}^{N^f} \Gamma_c^e$ and $\bigcap_{e=1}^{N^f} \Gamma_c^e = \emptyset$. These elements (Γ_c^e) constitute a *contact frame*. The contact tractions are discretized over the contact frame as:

$$\mathbf{t}_c \simeq \hat{\mathbf{t}}_c = \sum_{i=1}^{N^f} \delta_{P_i} \lambda_i \tag{33}$$

where δ_{P_i} is the Dirac delta on each contact frame node i , and λ_i is the Lagrange multiplier on the node ($i = 1 \dots N^f$). In the same way, the gap (\mathbf{g}) is approximated as

$$\mathbf{g} \simeq \hat{\mathbf{g}} = \sum_{i=1}^{N^f} \delta_{P_i} \mathbf{k}_i \tag{34}$$

where \mathbf{k}_i is the nodal value. Therefore, taking into account (34), the discrete expression of equation (2) can be written as:

$$(\mathbf{k})_I = (\mathbf{k}_{go})_I + (\mathbf{d}^2)_I - (\mathbf{d}^1)_I \tag{35}$$

for every contact pair I . In the expression above, \mathbf{k} is the contact pairs gap vector and \mathbf{k}_{go} the initial geometrical gap and translation vector.

4.3 BEM-BEM coupling equations

Equation (32) can be written for contact problems as: $\mathbf{A}_x \mathbf{x} + \mathbf{A}_p \mathbf{p}_c = \mathbf{F}$, being \mathbf{x} the nodal unknowns vector that collects the external unknowns and the contact displacements; \mathbf{p}_c is the nodal contact tractions; \mathbf{A}_p is constructed with the columns of \mathbf{G} belonging to the contact nodal unknowns, and \mathbf{A}_x , with the columns of matrices \mathbf{H} and \mathbf{G} , corresponding to the exterior unknowns and the contact nodal displacements. So the BEM-BEM contact system can be expressed, according to [Rodríguez-Tembleque and Abascal (2010b)], as:

$$\begin{bmatrix} \mathbf{A}_x^1 & \mathbf{0} & \mathbf{A}_p^1 \tilde{\mathbf{C}}^1 & \mathbf{0} \\ \mathbf{0} & \mathbf{A}_x^2 & -\mathbf{A}_p^2 \tilde{\mathbf{C}}^2 & \mathbf{0} \\ (\mathbf{C}^1)^T & -(\mathbf{C}^2)^T & \mathbf{0} & \mathbf{C}_g \end{bmatrix} \begin{Bmatrix} \mathbf{x}^1 \\ \mathbf{x}^2 \\ \Lambda \\ \mathbf{k} \end{Bmatrix} = \begin{Bmatrix} \mathbf{F}^1 \\ \mathbf{F}^2 \\ \mathbf{C}_g \mathbf{k}_{go} \end{Bmatrix} \quad (36)$$

where vector Λ represents the nodal contact tractions, so that: $\mathbf{p}_c^1 = \tilde{\mathbf{C}}^1 \Lambda$ and $\mathbf{p}_c^2 = -\tilde{\mathbf{C}}^2 \Lambda$. The matrices \mathbf{C}^α ($\alpha = 1, 2$), were defined in [Rodríguez-Tembleque and Abascal (2010b)], and they allow to extract the solid Ω^α contact node displacements from \mathbf{x}^α and \mathbf{C}_g is a Boolean matrix also defined in [Rodríguez-Tembleque and Abascal (2010b)]. The first two rows on (36) represent the boundary element equations of each solid, and the third row, the kinematic contact equations. Expression (36) can be written in a more compact form as:

$$\mathbf{R}^1 \mathbf{x}^1 + \mathbf{R}^2 \mathbf{x}^2 + \mathbf{R}_\lambda \Lambda + \mathbf{R}_g \mathbf{k} = \bar{\mathbf{F}} \quad (37)$$

being the matrices \mathbf{R}^1 , \mathbf{R}^2 , \mathbf{R}_λ and \mathbf{R}_g , and vector $\bar{\mathbf{F}}$, the corresponding block matrices of system (36).

4.4 Contact restrictions

Contact restrictions (15) for every contact pair I can be expressed in a discrete form as:

$$(\Lambda_t)_I - \mathbb{P}_{\mathbb{E}_\rho}((\Lambda_t^*)_I) = \mathbf{0} \quad (\Lambda_n)_I - \mathbb{P}_{\mathbb{R}_-}((\Lambda_n^*)_I) = \mathbf{0} \quad (38)$$

where augmented contact variables are defined as: $(\Lambda_t^*)_I = (\Lambda_t)_I - r_t \mathbb{M}^2(\dot{\mathbf{k}}_t)_I$ and $(\Lambda_n^*)_I = (\Lambda_n)_I + r_n (\mathbf{k}_n)_I$, and the value of ρ for the I pair: $\rho = |\mathbb{P}_{\mathbb{R}_-}((\Lambda_n^*)_I)|$.

4.5 Anisotropic wear equations

The wear depth for every instant or rotation ($g_w^{(k)}$) can be discretized over the contact frame, as a function of the nodal values as

$$g_w^{(k)} \simeq \hat{g}_w^{(k)} = \tilde{\mathbf{N}}\mathbf{w}^e \tag{39}$$

being $\tilde{\mathbf{N}}$ the shape functions matrix defined for the frame element Γ_c^e , and \mathbf{w}^e the nodal wear depth vector of element e . Therefore, the discrete form of kinematic equation (29) for I pair, at instant k , is

$$(\mathbf{k}^{(k)})_I = (\mathbf{k}_{go}^{(k)})_I + (\mathbf{d}^{2(k)})_I - (\mathbf{d}^{1(k)})_I + (\mathbf{C}_{gn}\mathbf{w}^{(k)})_I \tag{40}$$

where $\mathbf{w}^{(k)}$ is a vector which contains the contact pairs wear depth, and matrix \mathbf{C}_{gn} is constituted using the \mathbf{C}_g columns which affect the normal gap of contact pairs. The discrete expression of (27) can be written for I pair as

$$(\mathbf{w}^{(k)})_I = (\mathbf{w}^{(k-1)})_I + |(\Lambda_n^{(k)})_I| |(\mathbf{k}_t^k)_I - (\mathbf{k}_t^{(k-1)})_I|_i \tag{41}$$

where $\Lambda_n^{(k)}$ is a vector which contains the normal traction components of contact pairs at instant k .

5 Solution scheme

The quasi-static wear contact problem equations set (37–40) allow to compute the variables on instant or load step (k), $\mathbf{z}^{(k)} = [(\mathbf{x}^1)^T (\mathbf{x}^2)^T \Lambda^T \mathbf{k}^T \mathbf{w}^T]^T$, when the variables on previous instant are known. In this work $\mathbf{z}^{(k)}$ is computed using the following iterative Uzawa predictor-corrector scheme with index (n):

(I) Initialization: $\mathbf{z}^{(0)} = \mathbf{z}^{(k-1)}$.

(II) Predictor step, solve:

$$\begin{bmatrix} \mathbf{R}^1 & \mathbf{R}^2 & \mathbf{R}_g \end{bmatrix} \begin{bmatrix} \mathbf{x}^1 \\ \mathbf{x}^2 \\ \mathbf{k} \end{bmatrix}^{(n+1)} = -\mathbf{R}_\lambda \Lambda^{(n)} + \bar{\mathbf{F}}^{(k)} \tag{42}$$

being

$$\bar{\mathbf{F}}^{(k)} = \begin{bmatrix} \mathbf{F}^{1(k)} \\ \mathbf{F}^{2(k)} \\ \mathbf{C}_g \left(\mathbf{k}_g + \mathbf{k}_o^{(k-1)} + \Delta\mathbf{k}_o^{(n)} + \mathbf{C}_{gn}\mathbf{w}^{(k-1)} \right) \end{bmatrix} \tag{43}$$

(III) Corrector step, update the contact tractions $\Lambda^{(n+1)}$ for every contact pair I :

$$(\Lambda_n^{(n+1)})_I = \mathbb{P}_{\mathbb{R}_-} ((\Lambda_n^{(n)})_I + r_n (\mathbf{k}_n^{(n+1)})_I) \quad (44)$$

$$(\Lambda_t^{(n+1)})_I = \mathbb{P}_{\mathbb{E}_\rho} ((\Lambda_t^{(n)})_I - r_t \mathbb{M}^2 [(\mathbf{k}_t^{(n+1)})_I - (\mathbf{k}_t^{(k-1)})_I]) \quad (45)$$

being $\rho = |(\Lambda_n^{(n+1)})_I|$, and the resulting accumulated wear depth:

$$(\mathbf{w}^{(n+1)})_I = (\mathbf{w}^{(k-1)})_I + |(\Lambda_n^{(n+1)})_I| \|(\mathbf{k}_t^{(n+1)} - \mathbf{k}_t^{(k-1)})_I\|_i \quad (46)$$

(IV) Compute the error function: $\Psi(\Lambda^{(n+1)}) = \|\Lambda^{(n+1)} - \Lambda^{(n)}\|$.

- (a) If $\Psi(\Lambda^{(n+1)}) \leq \varepsilon$, the solution for the instant (k) is reached: $\mathbf{z}^{(k)} = \mathbf{z}^{(n+1)}$. Only in case the applied boundary condition is the external load j -component ($\mathbf{Q}_j^{(k)}$), before reaching the solution for instant (k), the resultant applied loads on the contact zone (Γ_c) have to be calculated:

$$\mathbf{Q}_j^{(n+1)} = \int_{\Gamma_c} \Lambda_j^{(n+1)} d\Gamma \quad (47)$$

- (a.1) If $|\mathbf{Q}_j^{(n+1)}| > |\mathbf{Q}_j^{(k)}| + \varepsilon_{load}$, modify $\Delta \mathbf{k}_o^{(n)}$ and return to (II).
(a.2) Otherwise, the solution for instant (k) is reached: $\mathbf{z}^{(k)} = \mathbf{z}^{(n+1)}$.
(b) Otherwise, return to (II) evaluating: $\Lambda^{(n)} = \Lambda^{(n+1)}$ and iterate until the convergence is reached.

After the solution at instant (k), $\mathbf{z}^{(k)}$, is reached, the solution for the next instant is achieved evaluating: $\mathbf{z}^{(k-1)} = \mathbf{z}^{(k)}$ and returning to (I).

The presented algorithm can be accelerated using a fictitious wear coefficient, what leads to a fictitious wear depth increment, reducing considerably the number of load cycles. This idea was proposed by [Strömberg (1997)] and it has been applied by [Rodríguez-Tembleque, Abascal, and Aliabadi (2011)] in fretting wear problems.

6 Numerical simulations

The boundary element formulation presented above allows to compute wear on different contact conditions. This is going to be applied to study the influence of anisotropy in two different kind of fretting wear problems.

6.1 Hertzian contact under gross slip

An elastic cylinder of radius $R = 6 \text{ mm}$ and thickness $e = 1 \text{ mm}$ over an elastic $e \times 2L \times L$ block ($L = 3 \text{ mm}$) is under a constant normal load per unit length, $F = 18.5 \text{ N/mm}$, and a tangential displacement stroke amplitude of $g_o = 50 \text{ }\mu\text{m}$ (see Fig.3(a)). The elastic modulus and Poisson's ratio of both the cylinder and the block are 200 GPa and 0.3 , respectively. Solids are discretized using 944 linear quadrilateral boundary elements, using 200 elements on the potential contact zone. Fig.3(b) show mesh details. Elements on the potential contact zone present a non-equidistant distribution on axis x_2 , as it is detailed in Fig.3(b).

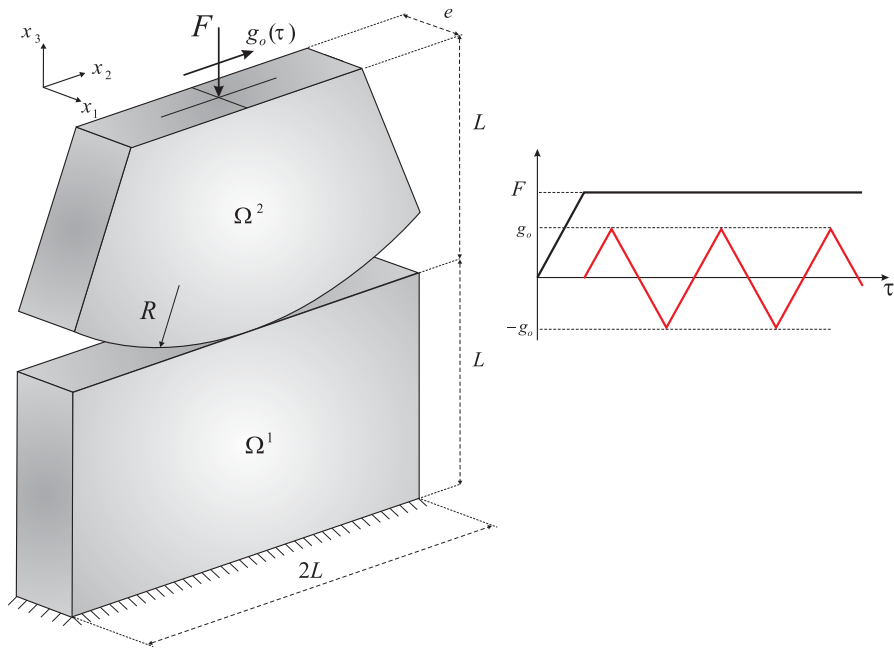
An orthotropic friction and wear laws are considered. Their coefficients in the tribological principal axis are: $\mu_1 = 0.4$, $\mu_2 = 0.8$, $i_1 = 2.5 \times 10^{-8} \text{ MPa}^{-1}$ and $i_2 = 5 \times 10^{-8} \text{ MPa}^{-1}$, being the ratio between the cylinder and the block wear intensities: $i_w^c/i_w^b = 2/3$. To study the influence of the anisotropic tribological properties in fretting wear problems, the principal axes orientation relative to the fretting direction are rotated: $\alpha = \{0^\circ, 45^\circ, 90^\circ\}$ (see Fig. 4).

The applied loads and boundary conditions leads to an Hertzian contact under gross slip, so wear is present in all the contact zone. The BE-predicted evolution of the contact pressure distribution and solids surface profiles for $\alpha = 0^\circ$, with increasing fretting wear cycles, are presented in Fig.5(a) and Fig.5(b), respectively, on middle plane $x_1 = 0$. The contact pressure distribution evolves with the changes of contact width from Hertz's distribution towards a uniform one.

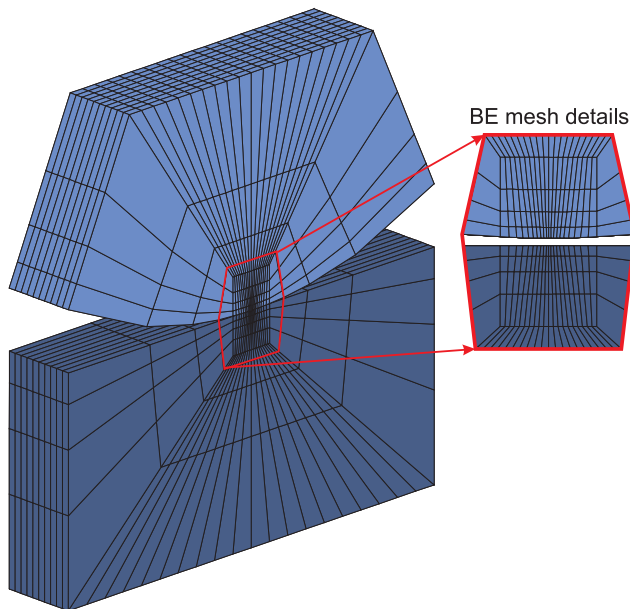
On Fig.6(a) and Fig.6(b) the BE half contact width and the peak normal contact pressure evolution, respectively, are presented for $\alpha = \{0^\circ, 45^\circ, 90^\circ\}$. The half contact width increases with the cycles in all cases, and consequently, the variation of peak pressure presents a decrease. The reduction is high during the first thousands cycles, and a much more gradual reduction over the subsequent cycles. We can see how the anisotropy on the tribological properties and the fretting orientation affect the mentioned contact variables. After 18000 cycles, a reduction of over thirty percent was observed in the half contact width for orientation $\alpha = 90^\circ$, relative to $\alpha = 0^\circ$, and an increment greater than forty percent in the peak pressure.

Influence of tribological properties principal axes orientation on wear evolution is also clear if the worn volume (Fig.7(a)) and wear depth (Fig.7(b)) evolutions are presented. A difference of forty percent was observed in the wear depth between orientation $\alpha = 0^\circ$ and $\alpha = 90^\circ$. Fig.8 shows the resulting wear depth distribution after 18000 cycles for: (a) $\alpha = 0^\circ$, (b) $\alpha = 45^\circ$ and (c) $\alpha = 90^\circ$.

The examples have been solved using the proposed algorithm, considering $r_{e_1} = 10^4$, $r_{e_2} = 8 \times 10^4$ and $r_n = 8 \times 10^4$ for the augmented Lagrangian, and $\varepsilon = 10^{-2}$ as a termination limit.



(a)



(b)

Figure 3: (a) Contact between two elastic bodies. (b) Boundary elements meshes.

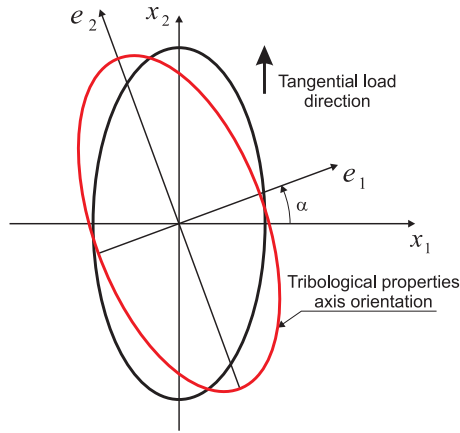


Figure 4: Tribological properties principal axes orientation relative to the fretting direction.

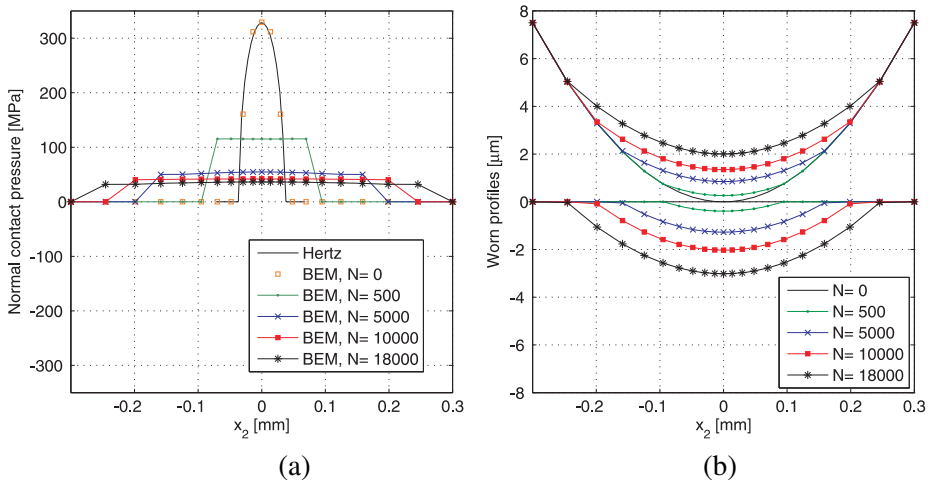


Figure 5: (a) Contact traction evolution on middle plane $x_1 = 0$ for different number of cycles. (b) Wear depth profiles evolution on $x_1 = 0$.

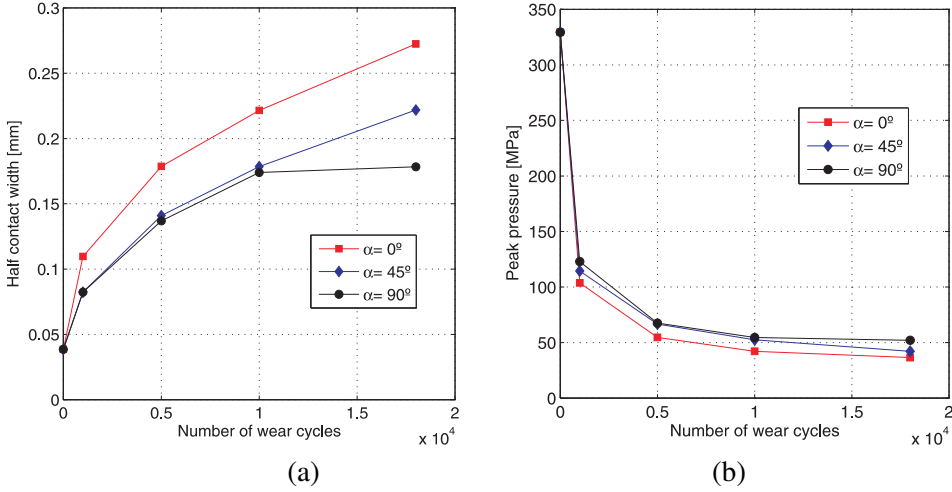


Figure 6: Influence of tribological properties principal axes orientation on: (a) the contact width and (b) the peak pressure evolution with the number of wear cycles.

6.2 Sphere-flat partial slip contact

This example presents a fretting problem between an elastic sphere of radius: $R = 50 \text{ mm}$ and an elastic half-space. The sphere is subjected to a normal displacement $g_{o,x_3} = -0.02 \text{ mm}$ and a repeated alternating tangential displacement $\mathbf{g}_{o,t} = 10 \text{ }\mu\text{m}$ (see Fig.9(a)).

The materials of the two contacting bodies are elastically similar: Young modulus $E^1 = E^2 = 10^4 \text{ MPa}$ and Poisson coefficients $\nu^1 = 0.3$ and $\nu^2 = 0.3$. For simplicity, the solids are approximated by elastic half-spaces, each one discretized using linear quadrilateral boundary elements. Fig.9(c) shows the meshes details, where the half-space characteristic dimension is $L = 1.3 \text{ mm}$. An orthotropic friction and wear law is considered, being $\mu_1 = 0.4$, $\mu_2 = 0.6$, $i_1 = 3.33 \times 10^{-7} \text{ MPa}^{-1}$ and $i_2 = 5 \times 10^{-7} \text{ MPa}^{-1}$.

The influence of the tangential load direction in the wear intensity can be observed in this sphere-flat with partial slip contact problem. The angle between the tangential load direction and x_1 direction is called α , and three values for α are considered: $\{0^\circ, 45^\circ, 90^\circ\}$. The wear depth evolutions with the number of cycles (N) is presented in Fig.10, for every fretting direction. A reduction greater than fifty percent can be observed in the wear depth for $\alpha = 90^\circ$ relative to $\alpha = 0^\circ$. Similar effects are observed in Fig.11, where the normal contact pressure evolutions

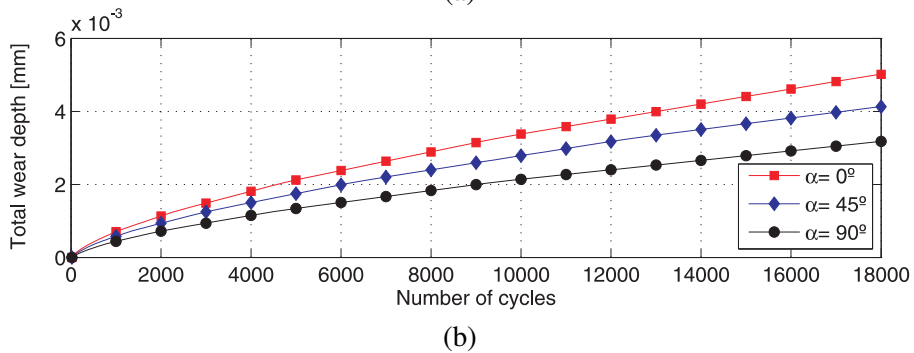
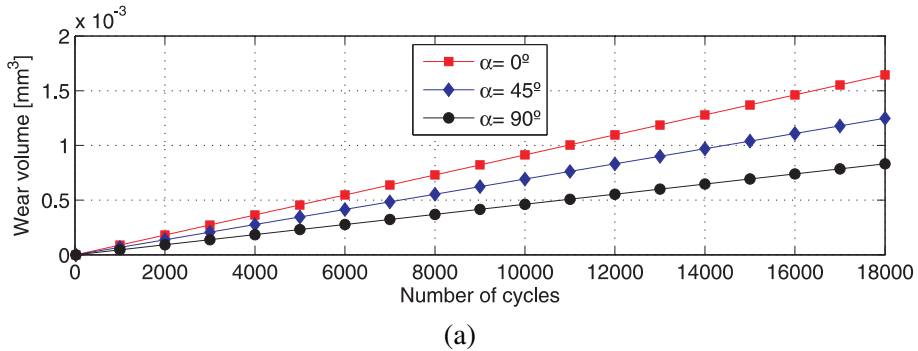


Figure 7: Influence of tribological properties principal axes orientation on: (a) worn volume, and (b) wear depth evolution.

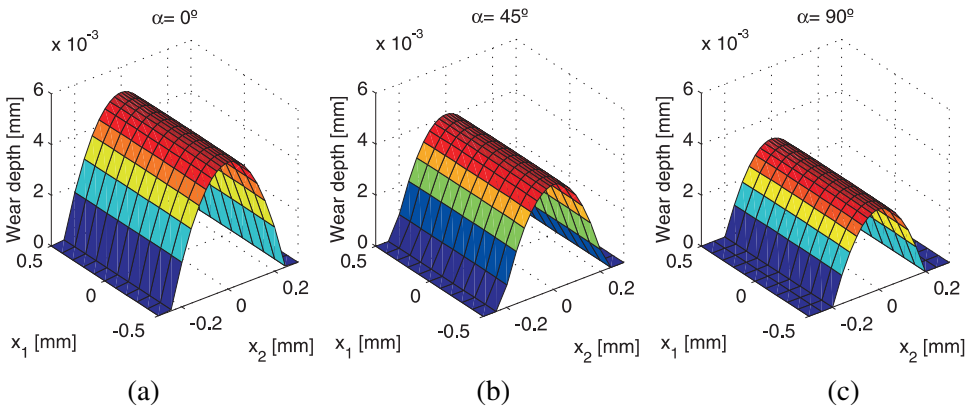
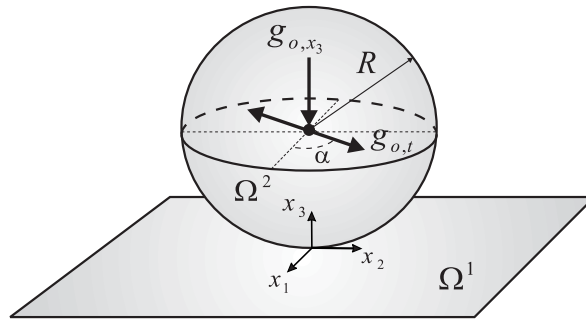
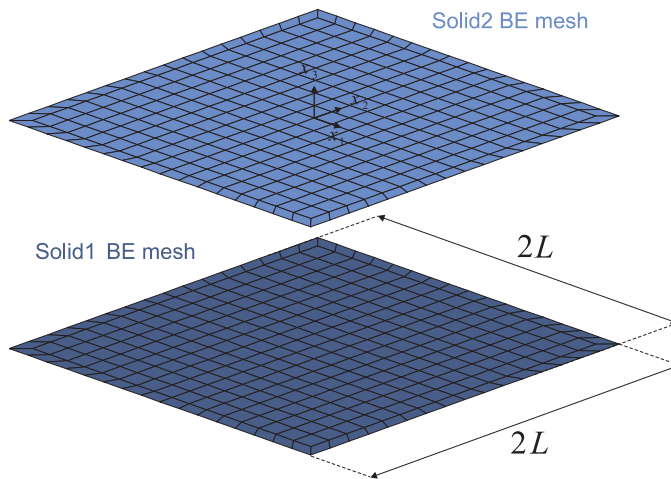


Figure 8: Resulting wear depth distribution after 18000 cycles for: (a) $\alpha = 0^\circ$, (b) $\alpha = 45^\circ$ and (c) $\alpha = 90^\circ$.



(a)



(b)

Figure 9: (a) Sphere-flat contact under tangential load direction relative to the tri-biological principal axes. (b) Boundary element mesh details for the half-space approximation.

are presented. Normal contact pressures evolve from an Hertzian distribution to a close complete normal contact traction distribution over the stick zone, and their maximum values are developed almost ten times greater than the maximum in the first cycles.

The importance of considering the anisotropic tribological properties is clear if we compare the maximum wear depth (Fig.12(a)) and normal contact pressure evolution (Fig.12(b)) with an isotropic case ($\mu_1 = \mu_2 = 0.6$ and $i_1 = i_2 = 5 \times 10^{-7} \text{ MPa}^{-1}$), being $\alpha = 45^\circ$. Figure 12(a) shows how the maximum wear depth for the anisotropic case is twice the maximum wear depth in the isotropic one, and an increment of fifty percent can be observed in the anisotropic maximum contact pressure over the isotropic one.

7 Summary and conclusions

This work presents a boundary element methodology for anisotropic wear simulation on 3D fretting problems. An augmented Lagrangian formulation, using an anisotropic frictional contact law, is proposed to model the contact problem, and an Uzawa predictor-corrector resolution scheme is presented to solve the non-linear equations set. The material loss of the bodies is modeled using an orthotropic wear law. Changes in the geometry of the solids are considered via the gap variable, which in case of small wear depth increments, avoids the remeshing of solids surfaces.

The BEM reveals to be a very suitable numerical method for this kind of solids mechanical interaction problem, considering only the degrees of freedom involved on the problem (those on the solids surfaces) and obtaining a very good approximation on contact tractions with a low number of elements. This fact is very interesting for the computational cost reductions on wear modeling, especially in 3D fretting problems, where a high number of load cycles are applied.

Finally, the methodology is applied to consider wear on different kinds of fretting contact conditions: gross-slip and partial slip, and on different kinds of 3D solids and surfaces. All these examples show the importance of considering wear in the contact process because of its influence in the contact variables (i.e. normal pressures are clearly modified). Furthermore, when the distribution of the asperities and hollows on the surfaces are not identical on every point it has to be considered an anisotropic friction and wear laws. In other case, we could over- or underestimate wear magnitudes and its distribution over the contact zone, as it was shown in the numerical examples.

Acknowledgement: This work was funded by the DGICYT of *Ministerio de*

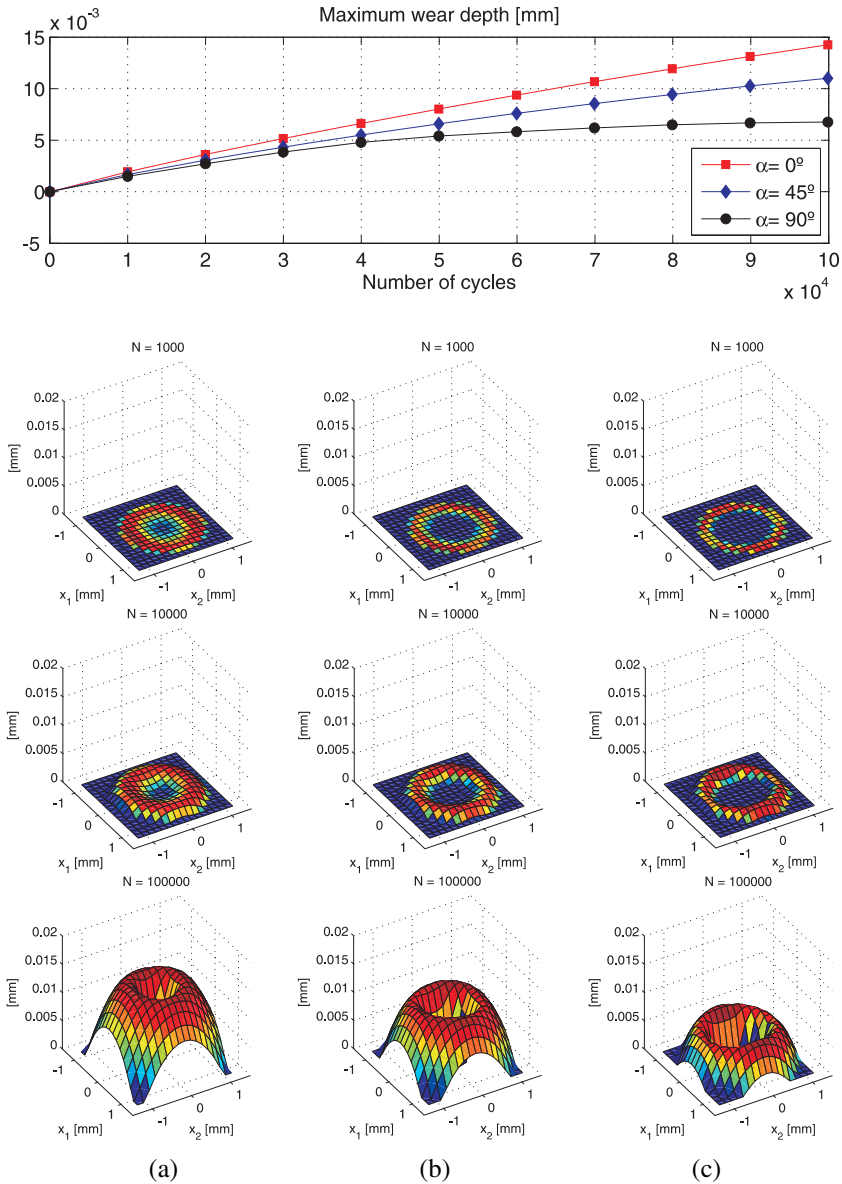


Figure 10: Wear depth evolution for: (a) $\alpha = 0^\circ$, (b) $\alpha = 45^\circ$ and (c) $\alpha = 90^\circ$.

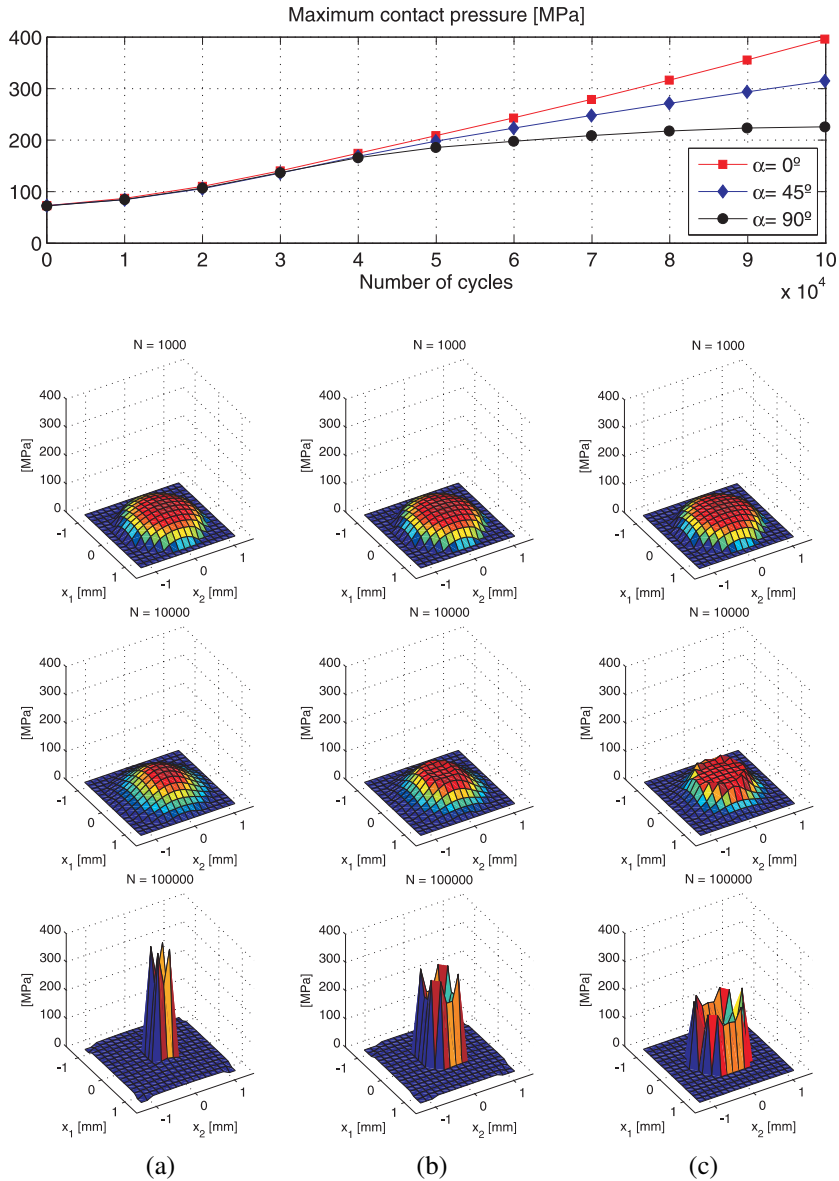


Figure 11: Normal contact pressure evolution for: (a) $\alpha = 0^\circ$, (b) $\alpha = 45^\circ$ and (c) $\alpha = 90^\circ$.

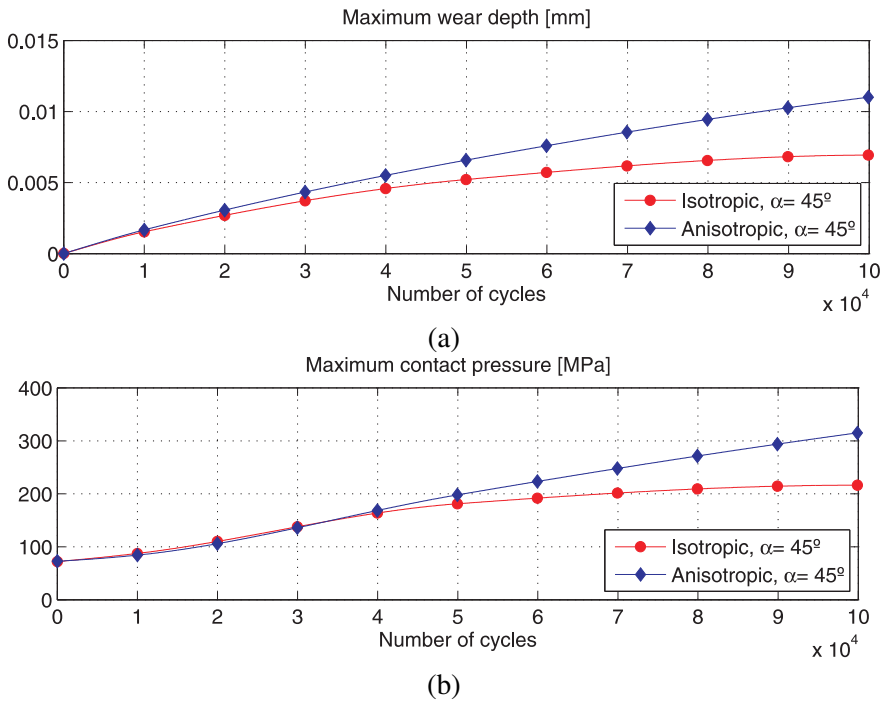


Figure 12: Comparison between an isotropic and anisotropic tribological properties maximum wear depth (a) and contact pressure (b) evolution.

Ciencia y Tecnología, Spain, research project DPI2010-19331, which it is co-funded with the European Regional Development Fund (ERDF), (Fondo Europeo de Desarrollo Regional, FEDER).

References

- Abascal, R.; Rodríguez-Tembleque, L.** (2007): Steady-state 3d rolling-contact using boundary elements. *Commun. Numer. Meth. Engng.*, vol. 23, pp. 905–920.
- Alart, P.; Curnier, A.** (1991): A mixed formulation for frictional contact problems prone to newton like solution methods. *Comput. Method. Appl. Mech. Eng.*, vol. 92, pp. 353–375.
- Aliabadi, M. H.** (2002): *The Boundary Element Method Vol2: Applications in Solids and Structures*. John Wiley & Sons.
- Archard, J. F.** (1953): Contact and rubbing of flat surfaces. *J. Appl. Phys.*, vol. 24, pp. 981–988.

- Brebbia, C. A.; Dominguez, J.** (1992): *Boundary Elements: An Introductory Course (second edition)*. WIT Press.
- Buczkowski, R.; Kleiber, M.** (1997): Elasto-plastic interface model for 3d-frictional orthotropic contact problems. *Int. J. Numer. Meth. Eng.*, vol. 40, pp. 599–619.
- Buczkowski, R.; Kleiber, M.** (2009): Statical models of rough surfaces for finite element 3d-contact analysis. *Arch. Comput. Methods.*, vol. 16, pp. 399–424.
- Christensen, P. W.; Klarbring, A.; Pang, J. S.; Strömberg, N.** (1998): Formulation and comparison of algorithms for frictional contact problems. *Int. J. Numer. Meth. Eng.*, vol. 42, pp. 145–173.
- Curnier, A.** (1984): A theory of friction. *Int. J. Solids Struct.*, vol. 7, pp. 637–647.
- de Saxcé, G.; Feng, Z. Q.** (1991): New inequality and functional for contact with friction: the implicit standard material approach. *Mech. Struct. Mach.*, vol. 19, pp. 301–325.
- Feng, Z. Q.; Hjjaj, M.; de Saxcé, G.; Mróz, Z.** (2006): Effect of frictional anisotropy on the quasistatic motion of a deformable solid sliding on a planar surface. *Comput. Mech.*, vol. 37, pp. 349–361.
- Feng, Z. Q.; Hjjaj, M.; de Saxcé, G.; Mróz, Z.** (2006): Influence of frictional anisotropy on contacting surfaces during loading/unloading cycles. *Int. J. Non-Linear Mech.*, vol. 41, pp. 936–948.
- González, J. A.; Abascal, R.** (1998): Using the boundary element method to solve rolling contact problems. *Engng. Anal. Bound. Elem.*, vol. 21, pp. 385–392.
- González, J. A.; Abascal, R.** (2000): An algorithm to solve coupled 2d rolling contact problems. *Int. J. Numer. Methods Eng.*, vol. 49, pp. 1143–1167.
- González, J. A.; Abascal, R.** (2002): Solving 2d transient rolling contact problems using the bem and mathematical programming techniques. *Int. J. Numer. Methods Eng.*, vol. 53, pp. 843–875.
- González, J. A.; Park, K. C.; Felippa, C. A.; Abascal, R.** (2008): A formulation based on localized lagrange multipliers for bem-fem coupling in contact problems. *Comput. Method. Appl. Mech. Eng.*, vol. 197, pp. 623–640.
- Goryacheva, I. G.; Rajeev, P. T.; Farris, T. N.** (2001): Mechanics of fretting fatigue. *ASME J. Tribol.*, vol. 123, pp. 848–856.
- Halaunbrenner, M.** (1960): Direction of the friction forces. *Wear*, vol. 3, pp. 421–425.

- Hartmann, S.; Oliver, J.; Weyler, R.; Cante, J. C.; Hernández, J. A.** (2009): A contact domain method for large deformation frictional contact problems. part 2: Numerical aspects. *Comput. Method. Appl. Mech. Eng.*, vol. 198, pp. 2607–2631.
- Hartmann, S.; Weyler, R.; Oliver, J.; Cante, J. C.; Hernández, J. A.** (2010): A 3d frictionless contact domain method for large deformation problems. *Computer Modeling in Engineering & Sciences*, vol. 55, pp. 211–270.
- Hills, D. A.; Nowell, D.** (1994): *Mechanics of Fretting Fatigue*. Kluwer Academic Publishers. Dordrecht, London.
- Hills, D. A.; Nowell, D.; Sackfield, A.** (1993): *Mechanics of Elastic Contact*. Butterworth-Heinemann, Oxford, UK.
- Hills, D. A.; Sackfield, A.; Paynter, R. J. H.** (2009): Simulation of fretting wear in halfplane geometries: Part i- the solution for long term wear. *ASME J. Tribol.*, vol. 131, pp. 31401–31404.
- Hjiaj, M.; de Saxcé, G.; Mróz, Z.** (2002): A variational inequality-based formulation of the frictional contact law with a non-associated sliding rule. *Eur. J. Mech. A/Solids.*, vol. 196, pp. 49–59.
- Hjiaj, M.; Feng, Z. Q.; de Saxcé, G.; Mróz, Z.** (2004): Three-dimensional finite element computations for frictional contact problems with non-associated sliding rule. *Int. J. Numer. Meth. Eng.*, vol. 60, pp. 2045–2076.
- Holm, R.** (1946): *Electric Contacts*. Almquist and Wiksells Akademiska Handböcker. Stockholm.
- Ireman, P.; Klarbring, A.; Strömberg, N.** (2003): A model of damage coupled to wear. *Int. J. Solids Struct.*, vol. 40, pp. 2957–2974.
- Ireman, P.; Klarbring, A.; Strömberg, N.** (2009): Gradient theory of damage coupled to frictional contact and wear, and its numerical treatment. *CMES: Computer Modeling in Engineering & Sciences*, vol. 52, pp. 125–158.
- Johansson, L.** (1994): Numerical simulation of contact pressure evolution in fretting. *ASME J. Tribol.*, vol. 116, pp. 247–254.
- Johnson, K. L.** (1985): *Contact Mechanics*. Cambridge University Press.
- Joli, P.; Feng, Z. Q.** (2008): Uzawa and newton algorithms to solve frictional contact problems within the bi-potential framework. *Int. J. Numer. Meth. Eng.*, vol. 73, pp. 317–330.
- Jones, R. S.; Papadopoulos, P.** (2006): Simulating anisotropic frictional response using smoothly interpolated traction fields. *Comput. Method. Appl. Mech. Eng.*, vol. 195, pp. 588–613.

Kim, T. W.; Moon, S. M.; Cho, Y. J. (2011): Prediction of fretting wear using boundary element method. *Tribol. Int.*, vol. 44, pp. 1571–1576.

Klarbring, A. (1992): *Mathematical Programming and Augmented Lagrangian Methods for Frictional Contact Problems*. Proceedings of Contact Mechanics International Symposium. Presses Polytechniques et Universitaires Romandes, Lausanne.

Klarbring, A. (1993): *Mathematical programming in contact problems*. Computational methods in contact mechanics.

Konyukhov, A.; Schweizerhof, K. (2006): Covariant description of contact interfaces considering anisotropy for adhesion and friction.: Part 2. linearization, finite element implementation and numerical analysis of the model. *Comput. Method. Appl. Mech. Eng.*, vol. 196, pp. 289–303.

Laursen, T. A. (2002): *Computational Contact and Impact Mechanics*. Springer, England.

Lee, C. Y.; Tian, L. S.; Bae, J. W.; Chai, Y. S. (2009): Application of influence function method on the fretting wear of tube-to-plane contact. *Tribol. Int.*, vol. 42, pp. 951–957.

Madge, J. J.; Leen, S. B.; Shipway, I. R. M. P. H. (2007): Contact-evolution based prediction of fretting fatigue life: Effect of clip amplitude. *Wear.*, vol. 262, pp. 1159–1170.

McColl, I. R.; Ding, J.; Leen, S. B. (2004): Finite element simulation and experimental validation of fretting wear. *Wear.*, vol. 256, pp. 1114–1127.

Michalowski, R.; Mróz, Z. (1978): Associated and non-associated sliding rules in contact friction problems. *Archiwum Mechaniki Stosowanej*, vol. 30, pp. 259–276.

Minford, E.; Prewo, K. (1985): Friction and wear of graphite-fiber-reinforced glass matrix composites. *Wear.*, vol. 102, pp. 253–264.

Mróz, Z.; Stupkiewicz, S. (1994): An anisotropic friction and wear model. *Int. J. Solids Struct.*, vol. 31, pp. 1113–1131.

Nowell, D. (2010): Simulation of fretting wear in halfplane geometries: Part ii-analysis of the transient wear problem using quadratic programming. *ASME J. Tribol.*, vol. 131, pp. 21402–21409.

Oliver, J.; Hartmann, S.; Cante, J. C.; Weyler, R.; Hernández, J. A. (2009): A contact domain method for large deformation frictional contact problems. part 1: Theoretical basis. *Comput. Method. Appl. Mech. Eng.*, vol. 198, pp. 2591–2606.

- Paczelt, I.; Kucharski, S.; Mróz, Z.** (2012): The experimental and numerical analysis of quasi-steady wear processes for a sliding spherical indenter. *Wear.*, vol. 274-275, pp. 127–148.
- Paczelt, I.; Mróz, Z.** (2012): Solution of wear problems for monotonic and periodic sliding with p -version of the finite element method. *Comput. Meth. Appl. Mech. Eng.*, pg. In press.
- Pödra, P.; Andersson, S.** (1999): Finite element analysis wear simulation of a conical spinning contact considering surface topography. *Wear.*, vol. 224, pp. 13–21.
- Pödra, P.; Andersson, S.** (1999): Simulating sliding wear with finite element method. *Tribol. Int.*, vol. 32, pp. 71–81.
- Rabinowicz, E.** (1957): Directional effects in friction. *Nature*, vol. 179, pp. 1073.
- Rabinowicz, E.** (1995): *Friction and Wear of Materials, second ed.* Wiley. New York.
- Rodríguez-Tembleque, L.; Abascal, R.** (2010): A 3d fem-bem rolling contact formulation for unstructured meshes. *Int. J. Solids Struct.*, vol. 47, pp. 330–353.
- Rodríguez-Tembleque, L.; Abascal, R.** (2010): A fem-bem fast methodology for 3d frictional contact problems. *Comput. Struct.*, vol. 88, pp. 924–937.
- Rodríguez-Tembleque, L.; Abascal, R.** (2012): Fast fe-bem algorithms for orthotropic frictional contact. *Int. J. Numer. Meth. Eng.*, vol. Submitted.
- Rodríguez-Tembleque, L.; Abascal, R.; Aliabadi, M. H.** (2010): A boundary element formulation for wear modeling on 3d contact and rolling-contact problems. *Int. J. Solids Struct.*, vol. 47, pp. 2600–2612.
- Rodríguez-Tembleque, L.; Abascal, R.; Aliabadi, M. H.** (2011): A boundary element formulation for 3d fretting-wear problems. *Engng. Anal. Bound. Elem.*, vol. 35, pp. 935–943.
- Sfantos, G. K.; Aliabadi, M. H.** (2006): Application of bem and optimization technique to wear problems. *Int. J. Solids Struct.*, vol. 43, pp. 3626–3642.
- Sfantos, G. K.; Aliabadi, M. H.** (2006): A boundary element sensitivity formulation for contact problems using the implicit differentiation method. *Engng. Anal. Bound. Elem.*, vol. 30, pp. 22–30.
- Sfantos, G. K.; Aliabadi, M. H.** (2006): Wear simulation using an incremental sliding boundary element method. *Wear.*, vol. 260, pp. 1119–1128.
- Sfantos, G. K.; Aliabadi, M. H.** (2007): A boundary element formulation for three-dimensional sliding wear simulation. *Wear.*, vol. 262, pp. 672–683.

Strömberg, N. (1997): An augmented lagrangian method for fretting problems. *Eur. J. Mech. A. Solids.*, vol. 16, pp. 573–593.

Strömberg, N. (1999): A newton method for three-dimensional fretting problems. *Int. J. Solids Struct.*, vol. 36, pp. 2075–2090.

Strömberg, N.; Johansson, L.; Klarbring, A. (1996): Derivation and analysis of a generalized standard model for contact. *Int. J. Solids Struct.*, vol. 33, pp. 1817–1836.

Wriggers, P. (2002): *Computational Contact Mechanics*. West Sussex, England.

Zhang, H. W.; He, S. Y.; Li, X. S.; Wriggers, P. (2004): A new algorithm for numerical solution of 3d elastoplastic contact problems with orthotropic friction law. *Comput. Mech.*, vol. 34, pp. 1–14.

Zmitrowicz, A. (1989): Mathematical descriptions of anisotropic friction. *Int. J. Solids Struct.*, vol. 25, pp. 837–862.

Zmitrowicz, A. (1993): Constitutive equations for anisotropic wear. *Int. J. Engng. Sci.*, vol. 31, pp. 509–528.

Zmitrowicz, A. (1999): An equation of anisotropic friction with sliding path curvature effects. *Int. J. Solids Struct.*, vol. 36, pp. 2825–2848.

Zmitrowicz, A. (2006): Models of kinematics dependent anisotropic and heterogeneous friction. *Int. J. Solids Struct.*, vol. 43, pp. 4407–4451.

Zmitrowicz, A. (2006): Wear patterns and laws of wear. *J. Theor. Appl. Mech.*, vol. 44, pp. 219–253.

Zmitrowicz, A. (2010): Contact stress: a short survey of models and methods of computations. *Arch. Comput. Methods.*, vol. 80, pp. 1407–1428.